Controlling Substrate Binding to Fe4S4 Clusters through Remote Steric Effects

Citation: Brown, Alexandra C. and Daniel L. M. Suess. "Controlling Substrate Binding to Fe4S4 Clusters through Remote Steric Effects." Inorganic Chemistry 58, 8 (March 2019): 5273–5280 © 2019 American Chemical Society

As Published: http://dx.doi.org/10.1021/acs.inorgchem.9b00360

Publisher: American Chemical Society (ACS)

Persistent URL: https://hdl.handle.net/1721.1/128193

Version: Author's final manuscript: final author's manuscript post peer review, without publisher's formatting or copy editing

Controlling Substrate Binding to Fe_4S_4 Clusters through Remote Steric Effects

*Alexandra C. Brown, Daniel L. M. Suess**

Department of Chemistry, Massachusetts Institute of Technology, Cambridge, Massachusetts 02139

Abstract

The extraordinary reactivity exhibited by many Fe–S enzymes is due in large part to the influence of the protein scaffold on substrate binding and activation. In principle, the coordination chemistry of synthetic Fe–S clusters could similarly be controlled through remote steric effects. Toward this end, we report the synthesis of 3:1 site-differentiated $[Fe_4S_4]$ clusters ligated by *N*-heterocyclic carbene (NHC) ligands with variable steric profiles: IMes (1,3-dimesitylimidazol-2-ylidene) and I^iPr^{Me} (1,3-diisopropyl-4,5-dimethylimidazol-2-ylidene). Treatment of $(IMes)_3Fe_4S_4Cl$ with $NaBAr^F{}_4$ in ethereal solvents (Et_2O and THF) leads to the formation of an ether adduct, $[(IMes)_3Fe_4S_4(solv)][BAr^F{}_4]$; solvent can be displaced by addition of ^{t}BuNC to form the unusual mono-isocyanide adduct $[(IMes)_3Fe_4S_4(CN^tBu)][BAr^F{}_4]$. Carrying out the same reactions with the less sterically encumbered cluster $(I^iPr^{Me})_3Fe_4S_4Cl$ results in more typical reactivity: undesired ligand redistribution to form the homoleptic cluster $[(I^iPr^{Me})_4Fe_4S_4][BAr^F{}_4]$ and generation of the tri-isocyanide adduct $[(I^iPr^{Me})_3Fe_4S_4(CN^tBu)_3][BAr^F{}_4]$. The increased steric profile of the IMes ligands disfavors ligand redistribution and defines a binding pocket at the apical Fe, thereby enabling the generation of a coordinatively unsaturated and substitutionally labile Fe site. This method of controlling the coordination chemistry at the apical Fe site by modifying the

sterics of ligands bound to adjacent Fe sites complements existing strategies for generating site-differentiated Fe–S clusters and provides new opportunities to direct reactivity at cuboidal metalloclusters.

Introduction

Fe–S cluster enzymes catalyze a diverse array of reactions central to metabolism, human health, and the biogeochemical cycles of the elements.[1–4] In addition to their widespread utility in electron transfer, many Fe–S enzymes including radical *S*-adenosylmethionine enzymes,[4] enzymes involved in isoprenoid biosynthesis (IspG and IspH),[5] aconitase,[6] nitrogenase,[7] and [NiFe]-CO dehydrogenase[8] react directly with substrates. In these cases, the environment of the cluster is carefully tuned by the surrounding amino acid residues to enable reactivity that would otherwise be thermodynamically and kinetically unfavorable. Realizing this exquisite control over binding and reactivity in synthetic Fe–S clusters remains an important challenge both to model the chemistry of biological Fe–S clusters and to generate synthetic Fe–S cluster catalysts.[9] To localize cluster reactivity to one Fe site, 3:1 site-differentiated [Fe_4S_4] clusters have been reported that feature chelating thiolate ligands[10–19] or monodentate phosphine[20–22] and thiolate[23] ligands (Chart 1). However, in all cases, these ligands offer limited opportunities to modify the environment at the apical Fe site because their steric bulk is positioned away from its coordination sphere. This is illustrated in each case by the stability of the corresponding homoleptic or pseudo-homoleptic complexes (Chart 1); even the most encumbering ligands are unable to prevent binding of an additional bulky ligand to the apical Fe site.[10,20–23] The challenge of controlling substrate binding at the apical Fe in these clusters contrasts decades of advances in mononuclear transition-metal chemistry in which steric parameterization[24,25] and modification have enabled the isolation of reactive and coordinatively unsaturated species.

As part of our efforts to develop reactive Fe–S clusters in protein-like environments, we herein describe the design and preparation of 3:1 site-differentiated $[Fe_4S_4]^+$ clusters bound by *N*-heterocyclic carbene (NHC) ligands that are sufficiently encumbering to prevent homoleptic

Chart 1. Representative site-differentiated [Fe_4S_4] clusters and their (pseudo-)homoleptic counterparts

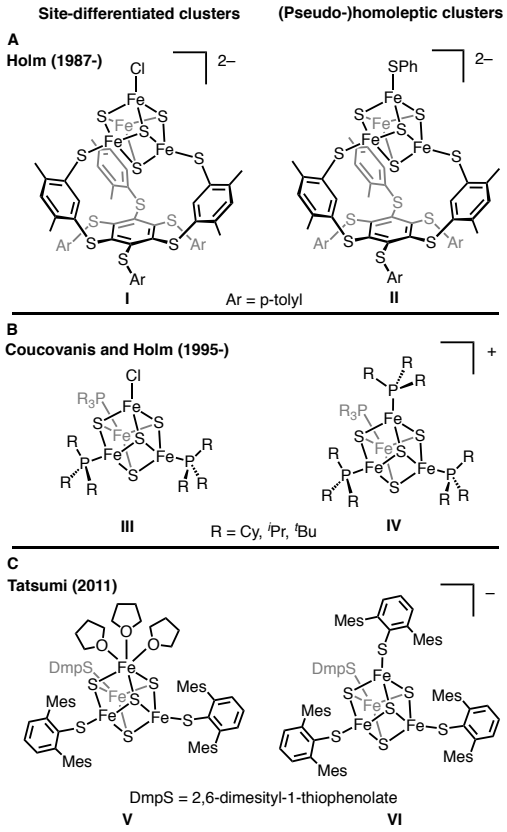

complex formation. We chose to study NHC ligands because of their strong σ-donor properties, which have resulted in their widespread use in chemical synthesis and catalysis. Previous studies have shown that NHCs can stabilize highly reduced Fe–S clusters: whereas $(PR_3)_4Fe_4S_4$ (R = Cy, ^{t}Bu, ^{i}Pr) clusters disproportionate to higher nuclearity clusters with concomitant loss of phosphine,[26] the analogous $(NHC)_4Fe_4S_4$ (NHC = 1,3-diisopropyl-4,5-dimethylimidazol-2-ylidene [I^iPr^{Me}] or 1,3-diethyl-4,5-dimethylimidazol-2-ylidene [IEt^{Me}]) clusters are thermally stable and can be isolated in pure form.[27,28] In comparison to other ligands for Fe–S clusters such as phosphines or thiolates, NHCs offer unique opportunities to modify the steric environment at the apical Fe site because their steric bulk is oriented toward the cluster core.[25,29] We demonstrate that in $(NHC)_4Fe_4S_4X$ clusters, increasing the length of the NHC through *N*,*N*'-diaryl substitution is key to forming and maintaining a substitutionally labile site at the apical Fe and that the

thermodynamics for substrate binding can be dramatically altered through these remote steric effects.

Experimental Section

General Considerations: Unless otherwise noted, all reactions were performed using standard Schlenk techniques or in an LC Technologies inert atmosphere glove box under an atmosphere of nitrogen (< 1 ppm O_2/H_2O). Glassware was dried in an oven at 160 °C prior to use. Molecular sieves (3 Å) and Celite® were activated by heating to 300 °C overnight under vacuum prior to storage under an atmosphere of nitrogen. Diethyl ether (Et_2O), benzene, pentane, and acetonitrile were degassed by sparging with argon, dried by passing through a column of activated alumina, and stored under an atmosphere of nitrogen over 3 Å molecular sieves. Tetrahydrofuran (THF) was distilled from sodium/benzophenone and stored under an atmosphere of nitrogen over 3 Å molecular sieves. C_6D_6 was degassed by three freeze–pump–thaw cycles and stored under an atmosphere of nitrogen over 3 Å activated molecular sieves. $(PCy_3)_3Fe_4S_4Cl$,[20] $NaBAr^F_4$,[30] IMes,[31,32], I^{i}Pr^{Me}[33] and $[(PCy_3)_4Fe_4S_4][BPh_4]$[26] were prepared according to literature procedures. *t*-butylisocyanide (^{t}BuNC) was degassed by three freeze-pump thaw cycles and stored under an atmosphere of nitrogen. PPh_4Cl was dried at 150 °C under vacuum for 16 h before use. All other reagents were purchased and used as received. NMR spectra were recorded on Bruker and Varian spectrometers. ^1H and $^{13}C\{^1H\}$ chemical shifts are given relative to residual solvent peaks. FT-IR samples were taken as thin films using a Bruker Alpha Platinum ATR spectrometer with OPUS software in a glovebox under an N_2 atmosphere. Diagnostic IR stretches are reported in the experimental details. EPR spectra were recorded on a Bruker EMX spectrometer at 9.37 GHz as frozen glasses. Simulations were performed using EasySpin[34] (5.2.21) in Matlab (R2017b). UV-vis spectra were taken on a Cary 50 spectrometer. Elemental analyses were performed at Robertson

Microlit laboratories or Midwest Microlab. X-ray structural determinations were performed at the MIT diffraction facility using a Bruker X8 diffractometer with an APEX II CCD detector or a Bruker D8 Venture diffractometer with a Photon2 CPAD detector. Diffraction data was collected, integrated, and corrected for absorption using Bruker APEX3 software and its associated modules (SAINT, SADABS, TWINABS). Structural solutions and refinements (on F^2) were carried out using SHELXT and SHELXL-2018 in ShelXle.[35] Ellipsoid plots and figures were made using Mercury.

(I^iPr^{Me})$_3$Fe$_4$S$_4$Cl (1): (PCy_3)$_3$Fe$_4$S$_4$Cl (204 mg, 0.166 mmol) was suspended in Et_2O (5 mL). A solution of I^iPr^{Me} (134 mg, 0.743 mmol) in Et_2O (2 mL) was added and the dark-brown suspension was stirred for 4 h. The black solid was collected on a frit and washed with Et_2O (3 x 10 mL). This procedure gave material of > 90% purity as determined by ^{1}H NMR spectroscopy (Fig. S1) and was used for further reaction studies. Yield: 123 mg (80 %). To remove trace PCy_3-containing products, the crude material could be recrystallized by mixing Et_2O (3 mL) into a benzene solution of **1** (50 mg in 1 mL) followed by storage at −35 °C overnight. The crystals could be washed quickly with benzene (5 × 1 mL) to obtain product of higher purity as judged by ^{1}H NMR spectroscopy (Fig. S2). Yield 4 mg (8%). ^{1}H NMR (400 MHz, C_6D_6, 293 K) δ 2.81 (36H, ^{i}Pr-CH_3), 4.81 (18H, backbone CH_3), 9.14 (6H, br, ^{i}Pr-CH). UV−vis (THF): λ_{max} (nm): 345 nm (ε = 12000 L/mol·cm). EPR: g_1 = 2.090, g_2 = 1.943, g_3 = 1.908 (toluene, 15 K, 9.37 GHz). Elemental analysis data were not obtained owing to the presence of trace impurities. X-ray quality crystals were grown by diffusion of Et_2O into fluorobenzene at ambient temperature.

(IMes)$_3$Fe$_4$S$_4$Cl (2): (PCy_3)$_3$Fe$_4$S$_4$Cl (1.00 g, 0.814 mmol) was dissolved in benzene (10 mL). A solution of IMes (810 mg, 2.66 mmol) in benzene (10 mL) was added dropwise and the dark-brown solution was stirred for 16 h. The mixture was then filtered through Celite, concentrated to

10 mL, and layered with pentane (40 mL). The mixture was allowed to stand for 2 h, then the black crystals were collected on a frit and washed with pentane (3 × 1 mL). Yield: 820 mg (77%) of pure compound as assessed by ^{1}H NMR (Fig. S3) and EPR (Fig. 2B) spectroscopies. ^{1}H NMR (500 MHz, C_6D_6, 293 K) δ 2.09 (36H, Mes *o*-C*H*$_3$), 2.26 (18H, Mes *p*-C*H*$_3$), 5.86 (6H, backbone CH), 6.91 (12H, Mes CH). UV−vis (THF): λ_{max} (nm): 324 nm (ε = 18000 L/mol·cm). EPR: g_1 = 2.122, g_2 = 1.964, g_3 = 1.937 (toluene, 15 K, 9.37 GHz). Evans method (C_6D_6, 293 K): 3.2 μ_B. Found: C, 57.99; H, 5.56; N, 6.42. Calc. for $C_{63}H_{72}N_6Fe_4S_4Cl$: C, 58.19; H, 5.58; N, 6.46. X-ray quality crystals were grown by diffusion of pentane into Et_2O at –35 °C.

Compound **2** can also be prepared without isolation of $(PCy_3)_3Fe_4S_4Cl$. $[(PCy_3)_4Fe_4S_4][BPh_4]$ (500 mg, 0.280 mmol) was dissolved in CH_2Cl_2 (5 mL). A solution of PPh_4Cl (140 mg, 0.373 mmol) in CH_2Cl_2 (2 mL) was added and the brown solution was stirred for 10 min. The mixture was then filtered through Celite and the solvent was removed *in vacuo*. The black solids were triturated with benzene to remove residual CH_2Cl_2 and a solution of IMes (280 mg, 0.822 mmol) in benzene (10 mL) was added. The brown solution was stirred for 16 h. The mixture was then filtered through Celite, concentrated to 5 mL, and layered with pentane (40 mL). The mixture was allowed to stand for 2 h, then the black crystals were collected on a frit and washed with pentane (3 × 1 mL). Yield: 303 mg (83 %). The spectroscopic data were identical to that described above.

$[(I^iPr^{Me})_4Fe_4S_4][BAr^F_4]$/$[(I^iPr^{Me})_4Fe_4S_4][BPh_4]$ (3) *Method 1*: To a solution of $NaBPh_4$ (18.6 mg, 0.054 mmol) and I^iPr^{Me} (9.9 mg, 0.055 mmol) in THF (2 mL) was added $(I^iPr^{Me})_3Fe_4S_4Cl$ (50 mg, 0.054 mmol) in benzene (2 mL). The solution was stirred for 1 h and filtered through Celite. The solvent was removed *in vacuo* to yield $[(I^iPr^{Me})_4Fe_4S_4][BPh_4]$ in >90% purity as determined by ^{1}H NMR and EPR spectroscopies (Fig. S4 and S22). Yield: 63 mg (84%). ^{1}H NMR (400 MHz, H_8-

THF, 293 K) δ 3.17 (48 H, ^{i}Pr-CH$_3$), 6.63 (24H, backbone CH$_3$), 6.83 (4H, [BPh$_4$]$^-$), 6.99 (8H, [BPh$_4$]$^-$), 7.50 (8H, [BPh$_4$]$^-$). ^{i}Pr–CH resonances were not observed. UV–vis (THF): λ_{max} (nm): 355 nm (ε = 12000 L/mol·cm). EPR: $g_{\|}$ = 2.114, $g_{\perp}$ = 1.903 (toluene/THF 10:1, 15 K, 9.37 GHz). Elemental analysis data were not obtained owing to the presence of trace impurities. X-ray quality crystals were grown by vapor diffusion of pentane into a fluorobenzene solution at ambient temperature.

The [BPh$_4$]$^-$ salt could be converted to the [BAr$^F_4$]$^-$ salt by dissolution in minimal THF (0.5 mL) followed by addition of NaBAr$^F_4$ (1 equiv) in Et$_2$O (4 mL). The solution was stirred for 5 min, then pumped down and extracted into C$_6$D$_6$ (0.5 mL). The ^{1}H NMR spectrum was identical to that of material generated by halide abstraction with NaBAr$^F_4$. ^{1}H NMR (400 MHz, C$_6$D$_6$, 293 K) δ 2.99 (48H, ^{i}Pr-CH$_3$), 6.15 (24H, backbone CH$_3$), 6.17 (6H, br, ^{i}Pr-CH), 7.68 (4H, [BAr$^F_4$]$^-$), 8.37 (8H, [BAr$^F_4$]$^-$).

Method 2: To a solution of [(PCy$_3$)$_4$Fe$_4$S$_4$][BAr$^F_4$] in C$_6$D$_6$ (0.5 mL) (generated *in situ* by anion exchange of [(PCy$_3$)$_4$Fe$_4$S$_4$][BPh$_4$] (20 mg, 0.011 mmol) in CH$_2$Cl$_2$ (1 mL) with NaBAr$^F_4$ (9.9 mg, 0.011 mmol) in Et$_2$O (1 mL), followed by extraction with Et$_2$O (1 mL) and filtration through Celite to remove NaBPh$_4$) was added a solution of I^{i}Pr^{Me} (8.1 mg, 0.045 mmol) in C$_6$D$_6$ (0.5 mL). A ^{1}H NMR spectrum recorded after 30 minutes of stirring was identical to that of material from method 1 (Fig. S6).

Method 3: Solutions of (I^{i}Pr^{Me})$_3$Fe$_4$S$_4$Cl (50.5 mg, 0.0388 mmol) in THF (4 mL) and NaBAr$^F_4$ (34.1 mg, 0.0385 mmol) in THF (4 mL) were cooled to –78 °C. The NaBAr$^F_4$ solution was added dropwise to the (I^{i}Pr^{Me})$_3$Fe$_4$S$_4$Cl solution and the resulting mixture was stirred for 2 h at –78 °C. The solution was then warmed to room temperature and the solvent removed *in vacuo*. The solids

were extracted with 3:1 C_6D_6/THF (1 mL), removing a black precipitate. The ^{1}H NMR spectrum was identical to that of material from method 1 (Fig. S7).

[(IMes)$_3$Fe$_4$S$_4$(THF)][BAr$^F_4$] (4): Solutions of (IMes)$_3$Fe$_4$S$_4$Cl (50.5 mg, 0.0388 mmol) in THF (4 mL) and NaBAr$^F_4$ (34.1 mg, 0.0385 mmol) in THF (4 mL) were cooled to –78 °C. The NaBAr$^F_4$ solution was added dropwise to the (IMes)$_3$Fe$_4$S$_4$Cl solution and the resulting mixture was stirred for 2 h at –78 °C. The solution was then warmed to room temperature and the solvent removed *in vacuo*. The dark-brown, sticky solids were redissolved in benzene (1 mL) and filtered through Celite to remove NaCl. This material was used as generated in > 90 % purity as determined by ^{1}H NMR (Fig. S8 and S9) and EPR (Fig. 2C) spectroscopies. ^{1}H NMR (400 MHz, C_6D_6, 293 K) δ 1.97 (36H, Mes *o*-C*H*$_3$), 2.24 (18H, Mes *p*-C*H*$_3$), 5.97 (6H, backbone CH), 6.80 (12H, Mes CH), 7.70 (4H, [BAr$^F_4$]$^-$), 7.75 (4H, br, THF), 8.44 (8H, [BAr$^F_4$]$^-$), 17.75 (4H, br, THF). EPR: g_1 = 2.116, g_2 = 1.942, g_3 = 1.911 (toluene/THF 10:1, 15 K, 9.37 GHz). Elemental analysis data were not obtained owing to the presence of trace impurities. X-ray quality crystals of **4**·Et$_2$O were grown by layering of pentane onto an Et$_2$O solution and storage at –35 °C overnight.

[(IMes)$_3$Fe$_4$S$_4$(CN^{t}Bu)][BAr$^F_4$] (5): A solution of (IMes)$_3$Fe$_4$S$_4$Cl (50 mg, 0.039 mmol) in THF (4 mL) and a solution of NaBAr$^F_4$ (34.1 mg, 0.0385 mmol) with ^{t}BuNC (10.5 mg, 0.126 mmol) in THF (4 mL) were cooled to –78 °C. The NaBAr$^F_4$/^{t}BuNC solution was added dropwise to the solution of **1** and the resulting mixture was stirred for 3 h at –78 °C. The solution was then warmed to room temperature and filtered through Celite. The solvent was removed *in vacuo* and the dark-brown solids were recrystallized by layering Et$_2$O (0.5 mL) with pentane (2 mL) to yield black crystals that were washed with pentane (3 x 1 mL). Yield: 68.3 mg (80 %) of pure compound as established by ^{1}H NMR (Fig. S10) and EPR (Fig. 2D) spectroscopies. ^{1}H NMR (400 MHz, C_6D_6, 293 K) δ 1.37 (9H, ^{t}BuNC) 2.07 (36H, Mes *o*-C*H*$_3$), 2.32 (18H, Mes *p*-C*H*$_3$), 6.22 (6H, backbone

CH), 6.94 (12H, Mes CH), 7.71 (4H, $[BAr^{F}_4]^-$), 8.46 (8H, $[BAr^{F}_4]^-$). FT-IR (thin film, cm^{-1}): 2121 (m, N-C stretch). UV–vis (THF): λ_{max} (nm): 360 nm (ε = 11000 L/mol·cm). EPR: g_1 = 2.177, g_2 = 1.972, g_3 = 1.944 (toluene/THF 10:1, 15 K, 9.37 GHz). Evans method (C_6D_6, 293 K): 3.2 μ_B. Found: C, 53.76; H, 4.49; N, 4.23. Calc. for $C_{100}H_{93}N_7Fe_4S_4BF_{24}$: C, 54.32; H, 4.24; N, 4.43. X-ray quality crystals were grown by layering pentane onto an Et_2O solution and storing at –35 °C overnight.

$[(I^iPr^{Me})_4Fe_4S_4(CN^tBu)_3][BAr^F_4]$ (6) and $[(I^iPr^{Me})_4Fe_4S_4][BAr^F_4]$ (3): A solution of $(I^iPr^{Me})_3Fe_4S_4Cl$ (7.2 mg, 0.0078 mmol) in benzene (1 mL) was added dropwise to a solution of $NaBAr^F_4$ (6.8 mg, 0.0077 mmol) and ^{t}BuNC (5.6 mg, 0.067 mmol) in Et_2O (1 mL). The solution was stirred for 1 h and filtered through Celite to remove dark solids. The solvent was removed *in vacuo*. A ^{1}H NMR spectrum of the crude material showed a mixture of **6** and **3** (Fig. S11). The resulting sticky oil was dissolved in toluene or Et_2O and studied immediately; **6** decomposes upon standing in Et_2O at RT. Yield (in situ, *vs.* a ferrocene internal standard): **6**: 0.0014 mmol (18 %); **3**: 0.0011 mmol (14 %). ^{1}H NMR (400 MHz, C_6D_6, 293 K) δ 0.52 (27H, ^{t}BuNC of **6**), 2.99 (48H, ^{i}Pr-CH_3 of **3**), 6.20 (24H, backbone CH_3 of **3**), 7.66 (4H, $[BAr^F_4]^-$), 8.30 (8H, $[BAr^F_4]^-$), 9.03 (36H, ^{i}Pr-CH_3 of **6**), 17.43 (18H, backbone CH_3 of **6**). FT-IR (thin film, cm^{-1}): 2132 (m, N–C stretch), 2074 (m, N–C stretch). EPR: **6**: g_{eff} = 8.583, 5.214, 4.242, (toluene/THF 10:1, 5 K, 9.37 GHz); **3**: $g_{\|}$ = 2.114, $g_{\perp}$ = 1.903 (toluene/THF 10:1, 15 K, 9.37 GHz). Elemental analysis data were not obtained owing to the instability of **6**.

Results and Discussion

Although no examples of $(NHC)_3Fe_4S_4X$ clusters have been reported,[36] we envisioned that substitution of the PCy_3 ligands in $(PCy_3)_3Fe_4S_4Cl$ with isolable NHCs could furnish the desired 3:1 site-differentiated $(NHC)_3Fe_4S_4Cl$ clusters. Indeed, reaction of $(PCy_3)_3Fe_4S_4Cl$ with three

equivalents of I^iPr^{Me} or IMes (IMes = 1,3-dimesitylimidazol-2-ylidene) gives the site-differentiated Fe–S clusters $(I^iPr^{Me})_3Fe_4S_4Cl$ (1) and $(IMes)_3Fe_4S_4Cl$ (2), respectively (Scheme 1). The ^1H NMR spectra (Fig. S1 and S3) show that both **1** and **2** have C_{3v} symmetry in solution and that the Fe–C bonds rotate freely at room temperature (RT). The structure of **1** was determined by X-ray diffraction (XRD) and shows the three NHCs oriented approximately coplanar to one another, leaving the coordination sphere of the apical Fe largely open (Fig. 1). In

Scheme 1. Preparation of NHC-ligated, 3:1 site-differentiated $[Fe_4S_4]^+$ clusters

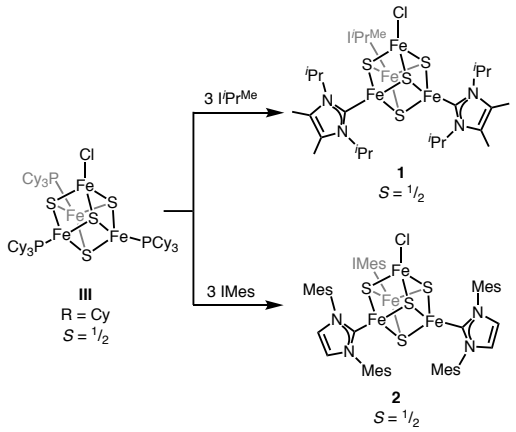

contrast, the IMes ligands in **2** are rotated vertically such that one set of mesityl groups is oriented toward the apical chloride (Fig. 1). The added length of IMes as compared to I^{i}Pr^{Me} forces the

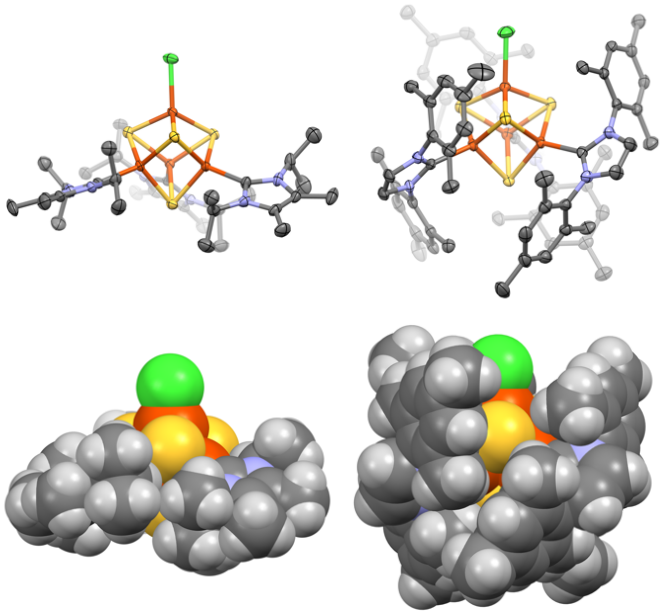

Figure 1. Thermal ellipsoid (50%; top) and space-filling (bottom) plots of **1** (left) and **2** (right) showing the increased steric protection of the apical Fe in **2** compared to **1**. Hydrogen atoms (top) and solvent molecules (top and bottom) are omitted for clarity. Color scheme: Fe (orange), S (yellow), Cl (green), N (blue), C (dark-grey), and H (light-grey).

NHCs to be more aligned with the molecule's pseudo-C_3 axis and engenders greater steric protection of the apical Fe site. The Fe–S distances within the clusters are highly variable (from 2.2567(8) to 2.321(1) Å for **1** and from 2.253(1) to 2.312(1) Å for **2**); such variability of Fe–S

bond lengths in $[Fe_4S_4]^+$ clusters has been previously observed and attributed to a shallow potential energy surface for core deformations.[21] This compressibility is exemplified by the structure of **2**, for which one molecule in the asymmetric unit displays the common elongated tetragonal distortion (two Fe_2S_2 rhombs with elongated bonds between them), while the other molecule displays less symmetric distortions. The clusters **1** and **2** display similar EPR spectra with $g_{iso} \sim 2$ (Fig. 2A and 2B) and similar UV/Vis spectra (Fig. S18 and S19). These findings are consistent

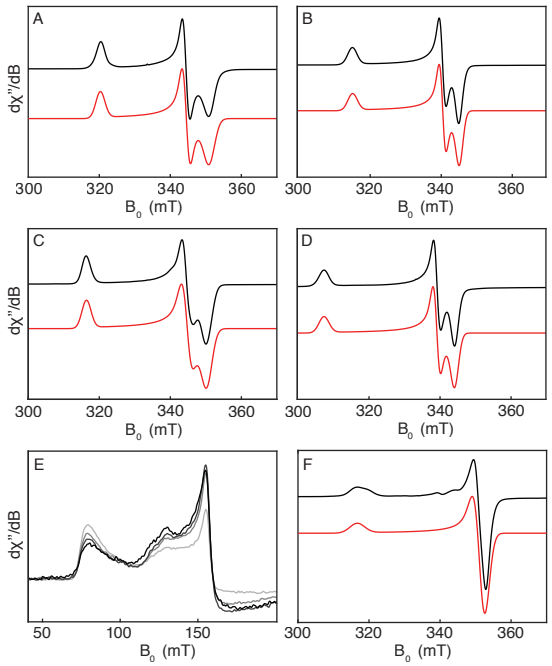

Figure 2: X-band EPR spectra (black) and simulations (red) of **1** (A, 15 K, 15 μW, g = [2.090 1.943 1.908]), **2** (B, 15 K, 126 μW, g = [2.122 1.964 1.937]), **4** (C, 15 K, 63 μW, g = [2.116 1.942 1.911]), **5** (D, 15 K, 63 μW, g = [2.177 1.973 1.944]), and the mixture formed upon reacting **1** with $NaBAr^F_4$ in the presence of excess ^{t}BuNC at low-field (E, showing the EPR spectra of **6** at 5 K (light gray), 8 K (medium gray), 10 K (dark gray), 15 K (black), 250 μW) and mid-field (F, showing the EPR spectrum of **3** at 15 K, 250 μW, g = [2.114 1.903 1.903], with minor impurities).

with the similar Tolman electronic parameters for I^iPr^{Me} and IMes (2047.8 and 2049.6, respectively[37]) and demonstrate that differences in the donor properties of I^iPr^{Me} and IMes minimally affect the electronic structures of the clusters. The EPR spectra of **1** and **2** are indicative of a ground S = ½ spin state; this spin state has been observed for all $[Fe_4S_4]^+$ clusters with

phosphine ligands and most synthetic and biological $[Fe_4S_4]^+$ clusters with thiolate ligands.[20,22,26,38–44]

Abstraction of the chloride ligand of **1** with sodium tetrakis[(3,5-trifluoromethyl)phenyl]borate ($NaBAr^F_4$) in tetrahydrofuran (THF) at –78 °C leads to formation of a dark-brown solution and an insoluble black precipitate (Scheme 2). The ^{1}H NMR spectrum of the soluble material shows bound I^iPr^{Me} and $[BAr^F_4]^-$ resonances in a 4:1 ratio. We therefore posited that the isolable product of this reaction was the homoleptic cluster $[(I^iPr^{Me})_4Fe_4S_4][BAr^F_4]$ (**3**), which was previously proposed to be generated upon electrochemical oxidation of $(I^iPr^{Me})_4Fe_4S_4$.[27] This assignment was confirmed by independent synthesis of **3** (treatment of **1** with $NaBAr^F_4$ in the presence of one equivalent of I^iPr^{Me}) and characterization by XRD (Fig. S26). The structure of **3** shows shorter Fe–C (2.060(7) Å) and Fe–S (2.29(3) Å) bond lengths compared to those of the previously reported reduced $(I^iPr^{Me})_4Fe_4S_4$ complex (2.11(2) and 2.33(2) Å, respectively).[27] A decrease of Fe–C and Fe–S bond lengths upon oxidation is also observed for the $[Fe_4S_4]^0$ and $[Fe_4S_4]^+$ clusters, $[Fe_4S_4(CN)_4]^{4-}$ and $[Fe_4S_4(CN)_4]^{3-}$.[45]

In contrast, treatment of **2** with $NaBAr^F_4$ in THF at –78 °C leads to the formation of one major product in approximately 90% purity (Scheme 2). The ^{1}H NMR spectrum of the product in

Scheme 2. Studies of chloride abstraction from **1** and **2**

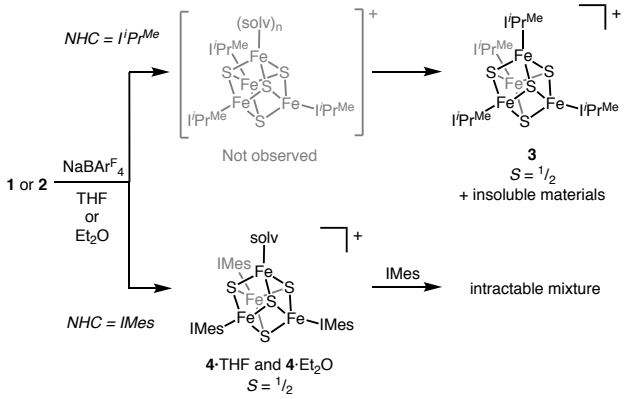

C_6D_6 displays a ratio of 3:1 between the bound IMes and $[BAr^F{}_4]^-$ resonances and broadened resonances corresponding to excess THF at 3.6 and 1.7 ppm, suggesting the formation of a THF adduct (**4**•THF). Lyophilizing samples from benzene to remove excess THF resulted in the appearance of two resonances at 17.73 and 7.86 ppm that each integrate for four protons relative to the IMes resonances and are assigned to a bound THF ligand (Fig. S9). The EPR spectrum of **4**•THF is rhombic with *g*-values that are similar to those of **2** (Fig. 2C). Single crystals grown in Et_2O layered with pentane were studied by XRD and confirmed the structure of **4**•Et_2O (Fig. 3) in which Et_2O is ligated to the apical Fe site. The pseudo-C_3 arrangement of the mesityl groups is similar to that in **2,** in which the mesityl groups form a well-defined cavity around the apical Fe site.

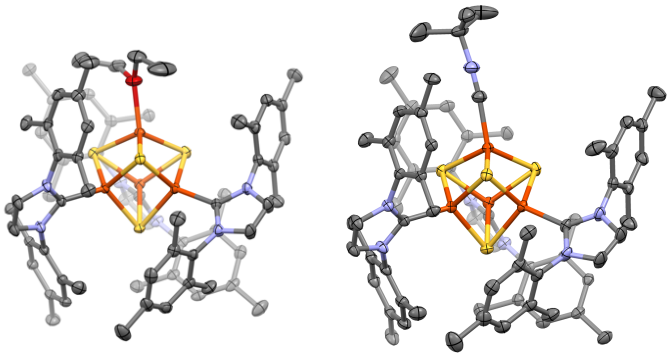

Figure 3. Thermal ellipsoid plots (50%) of **4**•Et_2O (left) and **5** (right). Hydrogen atoms, solvent molecules, and anions have been omitted for clarity. Color scheme: Fe (orange), S (yellow), O (red), N (blue), and C (dark gray).

Although **1** readily undergoes ligand redistribution following halide abstraction, the analogous redistribution of ligands from **4** to generate $[(IMes)_4Fe_4S_4][BAr^F{}_4]$ is disfavored; formation of the homoleptic cluster is not observed upon treatment of **2** with $NaBAr^F{}_4$, and attempted generation of $[(IMes)_4Fe_4S_4][BAr^F{}_4]$ by reaction of **4** with IMes leads to an intractable mixture. The steric bulk of IMes—particularly its length, owing to the *N*,*N*'-dimesityl

substituents—stabilizes **4** with respect to rearrangement reactions and allows for the generation of a complex with a labile coordination site.

We next sought to determine if the IMes ligands in **4** exert sufficient steric pressure at the apical Fe site to prevent formation of a coordinatively saturated, octahedral geometry upon substitution of the ether ligand with one or more strong-field ligands. We elected to study isocyanide binding because isocyanides are isoelectronic to N_2 and CO (substrates for synthetic and biogenic Fe–S clusters) and because of the strong driving force for binding three equivalents of isocyanide to generate a valence-localized, low-spin Fe^{2+} site: all reported examples of isocyanide binding to $[Fe_4S_4]$ clusters demonstrate that binding three isocyanides is more favorable than binding one or two (e.g. Scheme 3A).[46–51] We therefore expected that if sterically feasible, the apical Fe in **4** would also bind three equivalents of isocyanide. On the other hand, if the IMes

Scheme 3. Studies of isocyanide binding to (A) $[(LS_3)Fe_4S_4Cl]^{2-}$ and (B) **1** and **2**

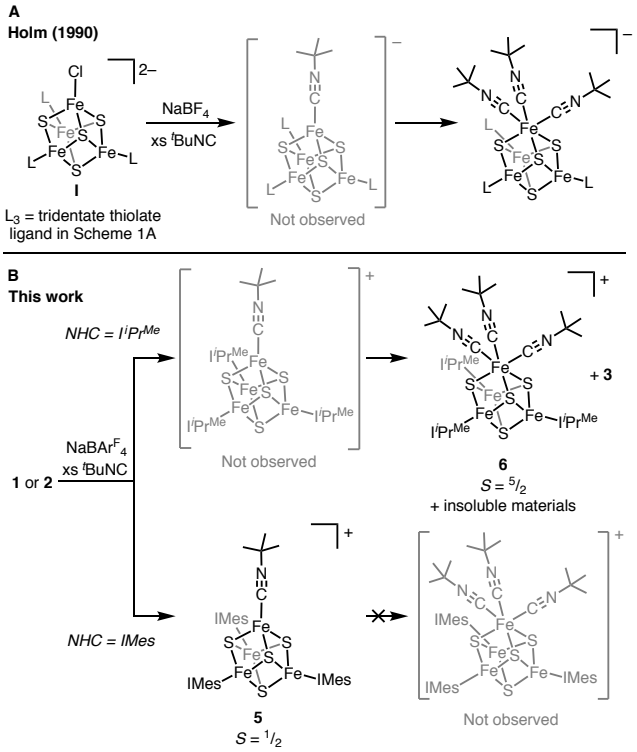

ligands impart sufficient steric pressure at the unique Fe site, only one isocyanide would bind, maintaining the apical Fe in a local high-spin configuration. Thus, we used isocyanide binding to test the hypothesis that the thermodynamics of ligand binding could be controlled through remote steric effects.

Addition of $NaBAr^F_4$ to **2** in the presence of excess ^{t}BuNC at –78 °C or addition of excess ^{t}BuNC to **4**•THF leads to the formation of a single product with an $S = {}^1/_2$ ground state (Scheme 3B, Fig. 2D). In addition to the IMes-derived resonances, the ^{1}H NMR spectrum of the product displays a singlet integrating for 9 protons at 1.36 ppm that we assign to a bound ^{t}BuNC ligand (Fig. S10). Together, these observations suggest that only one equivalent of ^{t}BuNC is bound, such that the apical Fe remains tetrahedral and high-spin (Fig. S25). An XRD experiment confirmed the assignment of this product as $[(IMes)_3Fe_4S_4(CN^tBu)][BAr^F_4]$ (**5**; Fig. 3). Consistent with the tetrahedral Fe geometry and high-spin state, the Fe–C bond is long (1.972(2) Å) compared to those of other Fe–S cluster isocyanide complexes (Fe–C (avg.): 1.84(3) Å), all of which adopt a local low-spin configuration.[46–50] Outside of its unprecedented nature in the Fe–S cluster literature, **5** is an uncommon example of a structurally characterized, terminal Fe isocyanide complex with a high-spin ground state.[52–56]

To determine if the binding of a single equivalent of ^{t}BuNC in **5** is indeed dictated by the steric pressure imposed by the IMes ligands, we carried out halide abstraction from **1** with $NaBAr^F_4$ in the presence of excess ^{t}BuNC (Scheme 3B). Although significant amounts of both insoluble materials and **3** were generated, an additional product was observed that is marked by its highly shifted ^{1}H NMR signals at 17.43 and 9.03 ppm (derived from the backbone C*H*$_3$ and isopropyl C*H*$_3$ groups of the I^iPr^{Me} ligands) as well as a new signal at 0.52 ppm (derived from ^{t}BuNC ligands). These resonances integrate in a 2:4:3 ratio, which suggests a cluster with three I^iPr^{Me}

ligands (18 and 36 H) and three ^{t}BuNC ligands (27 H; see Fig. S11). This new product decomposed to unidentified species after several hours at RT as evidenced by the concurrent disappearance of all three ^{1}H NMR resonances, and as such we were unable to characterize it by XRD. However, we further analyzed the initially formed mixture by IR (Fig. S17) and EPR spectroscopies (Fig. 2E and 2F). The reaction mixture shows absorbances in the IR spectrum assigned to bound isocyanide N–C stretches at 2132 and 2074 cm^{-1} (Fig. S17). EPR spectroscopy revealed one species with an $S = {}^5/_2$ spin state in addition to the $S = {}^1/_2$ signal for **3**. The ^{1}H NMR, IR, and EPR spectroscopic data are consistent with the formulation [(I^{i}Pr^{Me})$_3$Fe$_4$S$_4$(CN^{t}Bu)$_3$][BAr$^F{}_4$] (**6**); the $S = {}^5/_2$ spin state derives from valence isolation of a low-spin, apical Fe^{2+} site bound to an $S = {}^5/_2$ [Fe$_3$S$_4$]$^-$ cluster that has been previously identified in protein-bound [ZnFe$_3$S$_4$]$^+$ clusters (Fig. S25).[57,58] Variable temperature EPR spectroscopy (Fig. 2E) confirmed that the signals between $g_{eff} \sim 9$ and $g_{eff} \sim 4$ arise from a single species, and plotting the relative intensities as a function of temperature yields $D = 2.7(2)$ cm^{-1} (where D is the zero-field splitting; see ESI). This value is similar in magnitude but opposite in sign to those of the protein-bound [ZnFe$_3$S$_4$]$^+$ clusters in *D. gigas* ferredoxin II ($D = –2.7(5)$ cm^{-1}) and *P. furiousis* ferredoxin ($D = –2.7(5)$ cm^{-1}).[57,58]

That **6** is formed upon halide abstraction from **1** in the presence of ^{t}BuNC was expected based on previous studies of isocyanide binding to Fe–S clusters and is in contrast to the IMes-ligated clusters, for which **5** is generated with no evidence for the tri-isocyanide adduct [(IMes)$_3$Fe$_4$S$_4$(CN^{t}Bu)$_3$][BAr$^F{}_4$]. The IMes ligands in **5** prevent binding of additional equivalents of ^{t}BuNC despite the strong electronic driving force for binding three equivalents; binding three ^{t}BuNC ligands to the apical Fe would necessitate that the NHC ligands lie approximately coplanar to one another and perpendicular to the pseudo-C$_3$ axis of the molecule to allow the isocyanides to

project over the imidazolylidene rings. Although this coplanarity is accessible for I^{i}Pr^{Me}-ligated clusters, it is not possible for IMes-ligated clusters (Fig. 3).

Conclusions

We have demonstrated that the thermodynamic landscape for substrate binding to the apical Fe in a synthetic [Fe_4S_4] cluster can be dramatically altered through remote steric effects. Whereas 3:1 site-differentiated [Fe_4S_4]$^{+}$ clusters supported by the sterically unencumbering I^{i}Pr^{Me} ligand display typical reactivity towards ^{t}BuNC (binding three ^{t}BuNC ligands per labile Fe site), clusters supported by IMes bind only one ^{t}BuNC ligand to form **5**. Because of the steric pressure afforded by the IMes ligands, the apical Fe in **5** remains high-spin even in the presence of an excess of a strongly π-accepting ligand. Moreover, upon halide abstraction from **1**, the small I^{i}Pr^{Me} ligands do not prevent ligand redistribution and the undesired homoleptic cluster **3** is formed. In contrast, the steric bulk afforded by the *N*,*N*'-diaryl substituents of IMes in **2** allows for generation of a substitutionally labile, ether-ligated [Fe_4S_4]$^{+}$ cluster. The difference in reactivity between **1** and **2** is attributed to sterically imposed site-differentiation in **2**: the length of the NHC renders it unfavorable to form a homoleptic [$(NHC)_4Fe_4S_4$]$^{+}$ cluster upon abstraction of the apical chloride ligand. This strategy of imposing site-differentiation through remote steric effects complements established strategies of employing chelating ligands to generate site-differentiated Fe–S clusters and allows for control over the coordination environment of the apical Fe. We anticipate that the principles delineated in this work will allow for the isolation of Fe–S clusters in protein-like environments that exhibit new bonding and reactivity.

Supporting information available

NMR, IR and UV-Vis spectra, EPR simulation parameters and determination of *D* for **6**, spin coupling scheme for **6,** and crystallographic details.

Acknowledgements

We thank Drs. Peter Müller and Charlene Tsay for assistance with XRD experiments. This work was supported by fellowships for ACB from the National Science Foundation (Graduate Research Fellowship #1122374) and the Fannie and John Hertz Foundation.

References

(1) Flint, D. H.; Allen, R. M. Iron-Sulfur Proteins with Nonredox Functions. *Chem. Rev.* **1996**, *96* (7), 2315–2334.

(2) Beinert, H.; Holm, R. H.; Munck, E. Iron-Sulfur Clusters: Nature's Modular, Multipurpose Structures. *Science* **1997**, *277* (5326), 653–659.

(3) Johnson, D. C.; Dean, D. R.; Smith, A. D.; Johnson, M. K. Structure, Function and Formation of Biological Iron-Sulfur Clusters. *Annu. Rev. Biochem.* **2005**, *74*, 247–281.

(4) Broderick, J. B.; Duffus, B. R.; Duschene, K. S.; Shepard, E. M. Radical S-Adenosylmethionine Enzymes. *Chem. Rev.* **2014**, *114* (8), 4229–4317.

(5) Wang, W.; Oldfield, E. Bioorganometallic Chemistry with IspG and IspH: Structure, Function, and Inhibition of the [Fe_4S_4] Proteins Involved in Isoprenoid Biosynthesis. *Angew. Chemie - Int. Ed.* **2014**, *53* (17), 4294–4310.

(6) Beinert, H.; Kennedy, M. C.; Stout, C. D. Aconitase as Iron−Sulfur Protein, Enzyme, and Iron-Regulatory Protein. *Chem. Rev.* **1996**, *96* (7), 2335–2374.

(7) Burgess, B. K.; Lowe, D. J. Mechanism of Molybdenum Nitrogenase. *Chem. Rev.* **1996**, *96* (7), 2983–3012.

(8) Can, M.; Armstrong, F. A.; Ragsdale, S. W. Structure, Function, and Mechanism of the Nickel Metalloenzymes, CO Dehydrogenase, and Acetyl-CoA Synthase. *Chem. Rev.* **2014**, *114* (8), 4149–4174.

(9) Ohta, S.; Ohki, Y. Impact of Ligands and Media on the Structure and Properties of Biological and Biomimetic Iron-Sulfur Clusters. *Coord. Chem. Rev.* **2017**, *338*, 207–225.

(10) Stack, T. D. P.; Holm, R. H. Subsite-Differentiated Analogues of Biological $[4Fe\text{-}4S]^{2+}$ Clusters: Synthesis, Solution and Solid-State Structures, and Subsite-Specific Reactions. *J. Am. Chem. Soc.* **1988**, *110* (8), 2484–2494.

(11) Stack, T. D. P.; Holm, R. H. Subsite-Specific Functionalization of the $[4Fe\text{-}4S]^{2+}$ Analogue of Iron-Sulfur Protein Clusters. *J . Am. Chem. Soc.* **1987**, *109* (8), 2546–2547.

(12) Stack, T. D. P.; Weigel, J. A.; Holm, R. H. The Cavitand Concept in the Synthesis of Subsite-Differentiated Analogues of Biological $[4Fe\text{-}4S/Se]^{2+}$ Clusters: Cluster Capture Reactions, Ligand Conformational Analysis, and the Structure of a Trigonal $[4Fe\text{-}4Se]^{2+}$ Analogue. *Inorg. Chem.* **1990**, *29* (19), 3745–3760.

(13) Walsdorff, C.; Saak, W. A Preorganised Doubly Tripodal Hexathiol: Syntheses and Crystal Structures of Complexes with Two 3:1 Subsite-Differentiated Fe_4S_4 Clusters. *Chem. Commun.* **1997**, 1931–1932..

(14) Walsdorff, C.; Saak, W.; Pohl, S. A New Preorganized Tridentate Ligand Bearing Three Indolethiolate Groups. Preparation of 3 : 1 Subsite-Differentiated Fe_4S_4 Clusters. *J. Chem. Soc. Dalton Trans.* **1997**, 1857–1861.

(15) Barclay, J. E.; Evans, D. J.; Garcia, G.; Santana, M. D.; Torralba, M. C.; Yago, J. M. Binding of the $\{MoFe_3S_4\}^{3+}$ Core by a Tridentate Thiolate and Chemical Analogues of the Molybdenum Co-Ordination Environment in the Iron-Molybdenum Cofactor of Nitrogenase. *J. Chem. Soc. Dalton Trans.* **1995**, 1965–1971.

(16) Terada, T.; Wakimoto, T.; Nakamura, T.; Hirabayashi, K.; Tanaka, K.; Li, J.; Matsumoto, T.; Tatsumi, K. Tridentate Thiolate Ligands: Application to the Synthesis of the Site-

Differentiated [4Fe-4S] Cluster Having a Hydrosulfide Ligand at the Unique Iron Center. *Chem. Asian J.* **2012**, *7*, 920–929.

(17) Zhou, C.; Raebiger, J. W.; Segal, B. M.; Holm, R. H. The Influence of Net Charge on the Redox Potentials of Fe_4S_4 Cubane-Type Clusters in Aprotic Solvents. *Inorganica Chim. Acta* **2000**, *300–302*, 892–902.

(18) Weigel, J. A.; Holm, R. H. Intrinsic Binding Properties of a Differentiated Iron Subsite in Analogues of Native $[Fe_4S_4]^{2+}$ Clusters. *J. Am. Chem. Soc.* **1991**, *113* (11), 4184–4191.

(19) Ciurli, S.; Carrié, M.; Weigel, J. A.; Carney, M. J.; Stack, T. D. P.; Papaefthymiou, G. C.; Holm, R. H. Subsite-Differentiated Analogues of Native $[4Fe\text{-}4S]^{2+}$ Clusters: Preparation of Clusters with Five- and Six-Coordinate Subsites and Modulation of Redox Potentials and Charge Distributions. *J. Am. Chem. Soc.* **1990**, *112* (7), 2654–2664.

(20) Zhou, H.-C.; Holm, R. H. Synthesis and Reactions of Cubane-Type Iron−Sulfur−Phosphine Clusters, Including Soluble Clusters of Nuclearities 8 and 16. *Inorg. Chem.* **2003**, *42* (1), 11–21.

(21) Deng, L.; Majumdar, A.; Lo, W.; Holm, R. H. Stabilization of 3:1 Site-Differentiated Cubane-Type Clusters in the $[Fe_4S_4]^{1+}$ Core Oxidation State by Tertiary Phosphine Ligation: Synthesis, Core Structural Diversity, and $S = 1/2$ Ground States. *Inorg. Chem.* **2010**, *49* (23), 11118–11126.

(22) Tyson, M. A.; Demadis, K. D.; Coucouvanis, D. Uncharged Mixed-Ligand Clusters with the $[Fe_4S_4]^{+}$ and $[Fe_4S_4]^{2+}$ Cores. Synthesis, Structural Characterization, and Properties of the $Fe_4S_4X(^{T}Bu_3P)_3$ (X = Cl, Br, I) and $Fe_4S_4(SPh)_2(^{T}Bu_3P)_2$ Cubanes. *Inorg. Chem.* **1995**, *34* (18), 4519–4520.

(23) Ohki, Y.; Tanifuji, K.; Yamada, N.; Imada, M.; Tajima, T.; Tatsumi, K. Synthetic

Analogues of $[Fe_4S_4(Cys)_3(His)]$ in Hydrogenases and $[Fe_4S_4(Cys)_4]$ in HiPIP Derived from All-Ferric $[Fe_4S_4\{N(SiMe_3)_2\}_4]$. *PNAS* **2011**, *108* (31), 12635–12640.

(24) Tolman, C. A. Phosphorus Ligand Exchange Equilibriums on Zerovalent Nickel. Dominant Role for Steric Effects. *J. Am. Chem. Soc.* **1970**, *92* (10), 2956–2965.

(25) Gómez-Suárez, A.; Nelson, D. J.; Nolan, S. P. Quantifying and Understanding the Steric Properties of N-Heterocyclic Carbenes. *Chem. Commun.* **2017**, *53*, 2650–2660.

(26) Goh, C.; Segal, B. M.; Huang, J.; Long, J. R.; Holm, R. H. Polycubane Clusters: Synthesis of $[Fe_4S_4(PR_3)_4]^{1+,0}$ (R = Bu(t), Cy, Pr(i)) and $[Fe_4S_4]^0$ Core Aggregation upon Loss of Phosphine. *J. Am. Chem. Soc.* **1996**, *118* (47), 11844–11853.

(27) Deng, L.; Holm, R. H. Stabilization of Fully Reduced Iron-Sulfur Clusters by Carbene Ligation: The $[Fe_nS_n]^0$ Oxidation Levels (n = 4, 8). *J. Am. Chem. Soc.* **2008**, *130* (30), 9878–9886.

(28) Zhang, H.; Ouyang, Z.; Liu, Y.; Zhang, Q.; Wang, L.; Deng, L. (Aminocarbene)(Divinyltetramethyldisiloxane)Iron(0) Compounds: A Class of Low-Coordinate Iron(0) Reagents. *Angew. Chemie - Int. Ed.* **2014**, *53* (32), 8432–8436.

(29) Huang, J.; Schanz, H.-J.; Stevens, E. D.; Nolan, S. P. Stereoelectronic Effects Characterizing Nucleophilic Carbene Ligands Bound to the Cp*RuCl (Cp* = η^5-C_5Me_5) Moiety: A Structural and Thermochemical Investigation. *Organometallics* **1999**, *18* (12), 2370–2375.

(30) Yakelis, N. A.; Bergman, R. G. Safe Preparation and Purification of Sodium Tetrakis[(3,5-Trifluoromethyl) Phenyl]Borate ($NaBArF_{24}$): Reliable and Sensitive Analysis of Water in Solutions of Fluorinated Tetraarylborates. *Organometallics* **2005**, *24* (14), 3579–3581.

(31) Bantreil, X.; Nolan, S. P. Synthesis of *N*-Heterocyclic Carbene Ligands and Derived Ruthenium Olefin Metathesis Catalysts. *Nat. Protoc.* **2011**, *6* (1), 69–77.

(32) Hintermann, L. Expedient Syntheses of the *N*-Heterocyclic Carbene Precursor Imidazolium Salts IPr·HCl, IMes·HCl and IXy·HCl. *Beilstein J. Org. Chem.* **2007**, *3* (22).

(33) Kuhn, N.; Kratz, T. Synthesis of Imidazol-2-Ylidenes by Reduction of Imidazole-2(3H)-Thiones. *Synthesis* **1993**, *1993* (6), 561–562.

(34) Stoll, S.; Schweiger, A. EasySpin, a Comprehensive Software Package for Spectral Simulation and Analysis in EPR. *J. Magn. Reson.* **2006**, *178* (1), 42–55.

(35) Hübschle, C. B.; Sheldrick, G. M.; Dittrich, B. ShelXle: A Qt Graphical User Interface for SHELXL. *J. Appl. Crystallogr.* **2011**, *44* (6), 1281–1284.

(36) The Fe_4S_4 cluster [CAAC–H][(CAAC)$Fe_4S_4Br_3$] (CAAC = cyclic (alkyl)(amino)carbene) has been reported: Zhang, Y. Y.; Mei, T.; Yang, D.; Zhang, Y. Y.; Wang, B.; Qu, J. Synthesis and Reactivity of Thiolate-Bridged Multi-Iron Complexes Supported by Cyclic (Alkyl)(Amino)Carbene. *Dalton Trans.* **2017**, *46*, 15888–15896.

(37) Nelson, D. J.; Nolan, S. P. Quantifying and Understanding the Electronic Properties of N-Heterocyclic Carbenes. *Chem. Soc. Rev.* **2013**, *42* (16), 6723.

(38) Lane, R. W.; Wedd, A. G.; Gillum, W. O.; Laskowski, E. J.; Holm, R. H.; Frankel, R. B.; Papaefthymiou, G. C. Synthesis and Electronic Properties of the Tetranuclear Trianions $[Fe_4S_4(SR)_4]^{3-}$, Analogues of the 4-Fe Active Sites of Reduced Ferredoxins. *J. Am. Chem. Soc.* 1977, *99* (7), 2350–2352.

(39) Laskowski, E. J.; Frankel, R. B.; Gillum, W. O.; Papaefthymiou, G. C.; Renaud, J.; Ibers, J. A.; Holm, R. H. Synthetic Analogs of the 4-Fe Active Sites of Reduced Ferredoxins. Electronic Properties of the Tetranuclear Trianions $[Fe_4S_4(SR)_4]^{3-}$ and the Structure of

[$(C_2H_5)_3(CH_3)N]_3[Fe_4S_4(SC_6H_5)_4]$. *J. Am. Chem. Soc.* **1978**, *100* (17), 5322–5337.

(40) Stephan, D. W.; Papaefthymiou, G. C.; Frankel, R. B.; Holm, R. H. Analogues of the $[4Fe\text{-}4S]^+$ Sites of Reduced Ferredoxins: Structural and Spectroscopic Properties of $[(C_2H_5)_4N]_3[Fe_4S_4(S\text{-}p\text{-}C_6H_4Br)_4]$ in Crystalline and Solution Phases. *Inorg. Chem* **1983**, *22*, 1550–1557.

(41) Carney, M. J.; Papaefthymiou, G. C.; Spartalian, K.; Frankel, R. B.; Holm, R. H. Ground Spin State Variability in $[Fe_4S_4(SR)_4]^{3-}$. Synthetic Analogs of the Reduced Clusters in Ferredoxins and Other Iron-Sulfur Proteins: Cases of Extreme Sensitivity of Electronic State and Structure to Extrinsic Factors. *J. Am. Chem. Soc.* **1988**, *110* (18), 6084–6095.

(42) Carney, M. J.; Papaefthymiou, G. C.; Frankel, R. B.; Holm, R. H. Contribution from the Alternative Spin States in Synthetic Analogues of Biological [4Fe-4S]+ Clusters: Further Cases of Variable Ground States and the Structure of $(Et_4N)_3[Fe_4S_4(S\text{-}o\text{-}C_6H_4StBu)_4]$, Containing a Reduced Cluster with a Compressed Tetragonal Distortion; **1989**; *28*, 1497-1503.

(43) Carney, M. J.; Holm, R. H.; Papaefthymiou, G. C.; Frankel, R. B. Demonstration of Alternative Spin States in Clusters Containing the Biologically Relevant $[Fe_4S_4]^{1+}$ Core. *J. Am. Chem. Soc.* **1986**, *108* (12), 3519–3521.

(44) Venkateswara Rao, P.; Holm, R. H. Synthetic Analogues of the Active Sites of Iron−Sulfur Proteins. *Chem. Rev.* **2004**, *104* (2), 527–560.

(45) Scott, T. A.; Berlinguette, C. P.; Holm, R. H.; Zhou, H.-C. Initial Synthesis and Structure of an All-Ferrous Analogue of the Fully Reduced $[Fe_4S_4]^0$ Cluster of the Nitrogenase Iron Protein. *Proc. Natl. Acad. Sci* **2005**, *102* (28), 9741–9744.

(46) Harmjanz, M.; Saak, W.; Haase, D.; Pohl, S. Aryl Isonitrile Binding to $[Fe_4S_4]$ Clusters: Formation of $[Fe_4S_4]^+$ and $[\{Fe_4S_4\}_2]^{2+}$ cores. *Chem. Commun.* **1997**, 951–952.

(47) Weigel, J. A.; Holm, R. H.; Srivastava, K. K. P.; Day, E. P.; Münck, E. Isonitrile Binding to a Site-Differentiated Synthetic Analogue of Biological [4Fe-4S] Clusters: Equilibria, Magnetic Interactions and the Spin-Isolated [3Fe-4S] Cluster Fragment, and the Structure of a Low-Spin Iron(II) Subsite. *J. Am. Chem. Soc.* **1990**, *112* (22), 8015–8023

(48) Goh, C.; Weigel, J. A.; Holm, R. H. The [2:2] Site-Differentiated Clusters $[Fe_4S_4L_2(RNC)_6]$ Containing Two Low-Spin Iron(II) Sites. *Inorg. Chem.* **1994**, *33* (22), 4861–4868.

(49) Goh, C.; Nivorozhkin, A.; Yoo, S. J.; Bominaar, E. L.; Mu, E.; Holm, R. H. The Mixed-Valence Double-Cubanoid Cluster $[Fe_8S_{12}(Bu^tNC)_{12}]$: Synthesis , Structure , and Exchange Coupling of a New Structural Array of Four Fe (III) Sites. *Inorg. Chem* **1998**, *37* (12), 2926–2932.

(50) Cai, L.; Segal, B. M.; Long, J. R.; Scott, M. J.; Holm, R. H. Octanuclear Iron–Sulfur Clusters with Symmetrically Coupled Fe_4S_4 and Fe_4S_5 Cores. *J. Am. Chem. Soc.* **1995**, *117* (34), 8863–8864.

(51) Weigel, J. A.; Holm, R. H.; Surerus, K. K.; Munck, E. Spin-Isolation of the [3Fe-4S] Fragment of a [4Fe-4S] Cluster: Electronic Properties of the $[3Fe\text{-}4S]^0$ Cluster. *J. Am. Chem. Soc.* **1989**, *111* (26), 9246–9247.

(52) Bellows, S. M.; Brennessel, W. W.; Holland, P. L. Effects of Ligand Halogenation on the Electron Localization, Geometry and Spin State of Low-Coordinate (β-Diketiminato)Iron Complexes. *Eur. J. Inorg. Chem.* **2016**, *2016* (20), 3344–3355.

(53) Bellow, J. A.; Yousif, M.; Cabelof, A. C.; Lord, R. L.; Groysman, S. Reactivity Modes of

an Iron Bis(Alkoxide) Complex with Aryl Azides: Catalytic Nitrene Coupling vs Formation of Iron(III) Imido Dimers. *Organometallics* **2015**, *34* (12), 2917–2923.

(54) Chiang, K. P.; Barrett, P. M.; Ding, F.; Smith, J. M.; Kingsley, S.; Brennessel, W. W.; Clark, M. M.; Lachicotte, R. J.; Holland, P. L. Ligand Dependence of Binding to Three-Coordinate Fe(II) Complexes. *Inorg. Chem.* **2009**, *48* (12), 5106–5116.

(55) Esposito, V.; Solari, E.; Floriani, C.; Re, N.; Rizzoli, C.; Chiesi-Villa, A. Binding and Redox Properties of Iron(II) Bonded to an Oxo Surface Modeled by Calix[4]Arene. *Inorg. Chem.* **2000**, *39* (12), 2604–2613.

(56) Collins, T. J.; Fox, B. G.; Hu, Z. G.; Kostka, K. L.; Rickard, C. E. F.; Wright, L. J. High Valent Transition Metal Chemistry. Synthesis and Characterization of an Intermediate-Spin Iron(IV) Complex of a Strong π-Acid Ligand. *J. Am. Chem. Soc.* **1992**, *114* (22), 8724–8725.

(57) Surerus, K. K.; Münck, E.; Moura, I.; Moura, J. J. G.; LeGall, J. Evidence for the Formation of a $ZnFe_3S_4$ Cluster in Desulfovibrio Gigas Ferredoxin II. *J. Am. Chem. Soc.* **1987**, *109* (12), 3805–3807.

(58) Srivastava, K. K. P.; Surerus, K. K.; Conover, R. C. Moessbauer Study of Zinc-Iron-Sulfur $ZnFe_3S_4$ and Nickel-Iron-Sulfur $NiFe_3S_4$ Clusters in Pyrococcus Furiosus Ferredoxin. *Inorg. Chem.* **1993**, 32, 927–936.

TOC graphic

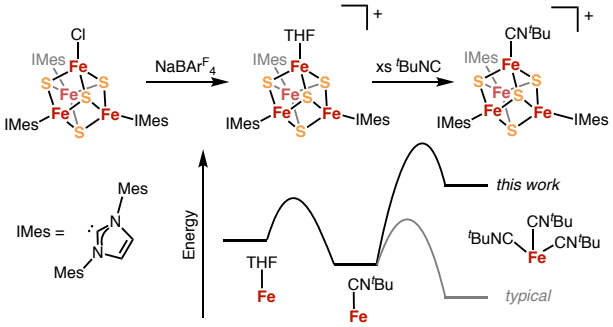

TOC synopsis: The extraordinary reactivity exhibited by many Fe–S enzymes is due in large part to the influence of the protein scaffold on substrate binding and activation. We report that ligation of synthetic, 3:1 site-differentiated [Fe_4S_4] clusters by sterically encumbering *N*-heterocyclic carbene (NHC) ligands enables the generation of a reactive Fe site and that steric pressure imbued by the NHCs can employed to rationally control substrate binding.